Artificial Intelligence in Agriculture 4 (2020) 74–80

Contents lists available at ScienceDirect

Artificial Intelligence in Agriculture

journal homepage: http://www.keaipublishing.com/en/journals/artificial-intelligence-in-agriculture/

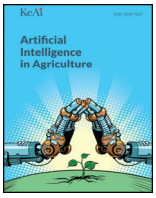

Precise in-situ characterization and cross-validation of the electromagnetic properties of a switched reluctance motor

Xiao Ling, Liang Gong *, Bingchu Li, Chengling Liu

The State Key Laboratory of Mechanical System and Vibration, School of Mechanical Engineering, Shanghai Jiao Tong University, China

ARTICLE INFO

Article history:
Received 1 November 2019
Received in revised form 14 May 2020
Accepted 14 May 2020
Available online 28 May 2020

Keywords:
Switched reluctance motor
Electromagnetic property characterization
Self-inductance
Incremental inductance
Flux linkage
In-situ measurement

ABSTRACT

The electrical-magnetic characteristics of a Switched Reluctance Motor (SRM) exhibit highly nonlinear relationship with respect to the rotor position and excitation current, which poses challenges for both precise static measurements and exact calculation of these properties in real-time control. To guarantee that an in-lab test result can be used in the application, firstly a measurement method is proposed to characterize the SRM's electromagnetic properties such as the flux linkage, magnetic co-energy, phase inductance and electromagnetic torque on the basis of an installed SRM control circuitry and half-bridge power converter. By this means the characterization process is equivalent to the online observation in its results. Secondly, a theoretical model is built to discriminate the physical meaning between the incremental inductance and the phase inductance, which is the origin of other relevant parameters. This helps to guide the correct utilization of the characterization result. Thirdly an in-situ cross-validation experimentation according to the magnetizing and demagnetizing status measurement verifies the feasibilities and accuracy of the proposed inductance measuring method, which avoid a dubious FEM-based comparison between the numerical calculation and experimental results. Cross-validation experiment shows that the proposed in-situ characterization scheme obtains an accurate full-range electromagnetic properties. The proposed methodology breaks the barrier between the in-lab measurement and on-line utilization of the SRM parameters, highlighting the merits that it completely includes the in-situ factors and replicates the operational scenario without the need of specifically designed instrumentation, which is especially suitable for rapid field characterization for high power motors.

1. Introduction

Due to simple and rugged motor construction, potentially low production cost, excellent torque/speed characteristics, high operating efficiency, and inherent fault tolerance, switched reluctance motors (SRMs) are emerging as an attractive drive unit ranging from modern electrical vehicles to high speed aircraft applications (Kamalakannan et al., 2011; Wen et al., 2013). In recent years, substantial research efforts have been devoted to various aspects of SRM such as speed regulation performance analysis, controller design and instrumentation, drive application, where the accurate knowledge of the SRM's electromagnetic characteristics is a defining property for all these cases.

Generally speaking, there are four principal parameters commonly used in high performance control of SRMs, namely the flux linkage ψ, magnetic co-energy W, phase inductance L and yielded electromagnetic torque T. Precise characterization of these electromagnetic properties is essential for SRM applications. For example, strategies in speed-position control, energy-efficient control and position sensor elimination control are highly dependent upon the accuracy of phase inductance (Yoo et al., 2009; Kjaer et al., 1995; Brauer et al., 2012; Yu et al., 2015). Soft computing of electromagnetic torque, instead of using a torque transducer, is extensively adopted for torque ripple minimization and noise reduction (Cai and Deng, 2012; Moron et al., 2012; Lee et al., 2012; Vujicic, 2012; Zeng et al., 2014). Flux linkage and magnetic co-energy are employed to realize high-performance four-quadrant operation (Goto et al., 2010; Wong et al., 2009; Cheok and Fukuda, 2002; Shin et al., 2005).

To date it remains challenging when precisely characterizing the parameters for control purpose since an SRM presents highly nonlinear characteristics due to the motor's doubly salient structure and its intentional operation in deep magnetic saturation for higher power density (Miller, 2001; Dowlatshahi et al., 2014). Moreover, a prominent subproblem associated is that the current accurate in-lab measurement results are rarely applicable in engineering, especially when the precise parameter evaluation is desired. The considerable errors between the in-lab characterization and field application stem from manufacturing and material variations from the prototype, neglect of phase mutual

* Corresponding author.
E-mail addresses: lingxiao@sjtu.edu.cn (X. Ling), gongliang_mi@sjtu.edu.cn (L. Gong), bchli@sjtu.edu.cn (B. Li), chlliu@sjtu.edu.cn (C. Liu).

https://doi.org/10.1016/j.aiia.2020.05.002

Nomenclature

A.C.	Alternating Current
COTS	Commercial Off-the-Shelf
D	Diode
D.C.	Direct Current
DSP	Digital Signal Processor
FPGA	Field Programmable Gate Array
i	Instantaneous Phase Current for Integration (A)
$\boldsymbol{I}$	Phase Current
IGBT	Insulated Gate Bipolar Transistor
$\boldsymbol{L}$	Phase Inductance
l	Incremental Inductance
R	Phase Resistance
S	Power Switch (IGBT)
SDRAM	Synchronous Dynamic Random Access Memory
SRM	Switched Reluctance Motor
$\boldsymbol{T}$	Electromagnetic Torque
u	Instantaneous Phase Voltage [V]
$\boldsymbol{W}$	Magnetic Co-energy
W_e	Input Electrical Energy
W_m	Mechanical Energy
Wf	Magnetic Field Energy
3D	Three Dimension

Greeks

$\boldsymbol{\Psi}$	Phase Flux linkage [*Wb*]
$\boldsymbol{\theta}$	rotor angular position [*rad*]
τ	Integration Time[s]

couplings, diverse winding copper and iron losses, and the chopping loss of power electronics devices. Therefore, although precisely characterizing the SRMs is extensively investigated (Zhang et al., 2010; Parreira et al., 2005; Wang et al., 2014) and gives perfect insight into the physics, there still exists a necessity to develop a rapid approach on characterizing the motors individually. In this sense the core issue is how to comprehensively replicate the operating scenario during the characterization process, where an in-situ characterization lends itself to serve this goal.

In engineering it deserves measurement innovations under several regards, including the convenience of experimental setup configuration, replication of the operating conditions and regimes, and security consideration for high power rating machines. Fortunately, these considerations can be encompassed via using the power and control circuitries readily equipped for a COTS motor product, given that the characterization abides by the operating state in all electrical tractor. With this original intention an in-situ method is proposed for precise measurement of SRM's electromagnetic properties in this paper. Additionally, an analytical solution is addressed to clarify the physical meaning of phase and incremental inductances, laying a theoretical foundation for different monitoring and control strategy designs for electrical motor. The verification of this characterization plays an importance role in reliably utilizing the result, and correspondingly a cross-validation approach is developed.

The organization of this paper is as follows. Section 2 proposes a precise SRM characterization model for an SRM, with an emphasis on discriminating the definition of phase and incremental inductance. Section 3 describes a COTS circuitry based in-situ characterizing approach for the motor, and the merits of this measuring method are also highlighted. Parameter measurement results and parameter characteristics are illustrated in Section 4, followed by a reliable in-situ cross-validation method. Some conclusions are given in Section 5.

2. Electrical model of the SRM

Determination of the magnetic characteristics can be realized numerically or experimentally. Measurement-based approaches show the merits of high precision, isolation of manufacturing variation and independence of prerequisite knowledge of material magnetics when compared to typical FEA numerical methods. In this section we present the theoretical fundamentals for motor characterization and clarify an important notation on the inductance, then propose a COTS apparatus based approach capable of easily characterizing the SRMs with high power ratings and the advantages are discussed.

2.1. Characterization fundamentals

Characterization of an SRM normally stems from measuring the flux linkage profile in one motor phase, and then other relevant properties can be derived using standard electrical machine theory. After blocking the rotor to a certain position, a pulse voltage is applied and the phase current responses are recorded and the measurement is repeated for different rotor positions to profile the motor properties according to the following electrical equations. By Faraday's law the voltage equation for one phase

$$u = Ri + \frac{d\psi(i\theta)}{dt} \tag{1}$$

where U is the instantaneous voltage across the terminals of a single phase of an SRM, i is the phase current, and R is the phase resistance. ψ is the flux linked per phase whose change rate with respect to time can be obtained.

The phase inductance L is defined by

$$\psi(i,\theta) = L(i,\theta)i \tag{2}$$

when given a fixed rotor position θ

$$\psi(i,\theta) = \int_0^{\tau} (u - Ri)dt \tag{3}$$

here when the phase current I traverses from zero to its maximum, the flux linkage can be computed accordingly. And the inductance profile can be calculated by partially deriving Eq. (3).

From the view angle of energy conservation, the input electrical energy W_e is equal to the sum of energy stored in the coil W_f and the energy converted into the mechanical work W_m.

$$W_e = W_f + W_m \tag{4}$$

We can define the stored magnetic energy W_f and its counterpart electromagnetic co-energy W as

$$W_f = \int_0^{\psi} i(\psi,\theta)\,\mathrm{d}\psi \tag{5}$$

$$W = \int_0^{I} \psi(i,\theta)\,\mathrm{d}i \tag{6}$$

The electromagnetic co-energy is introduced since it is common to express the electromagnetic torque in terms of current rather than flux linkage. And obviously there exist relations as

$$i\psi = W_f + W \tag{7}$$

and

$$\partial W_f \Big/ \partial\theta = -\partial W \Big/ \partial\theta \tag{8}$$

For the case of constant excitation, the incremental mechanical work is equal to the change rate of co-energy W, which is nothing but the complement of the field energy *Wf*. Hence the incremental mechanical work done can be written as

$$\delta W_m = \delta W \tag{9}$$

where

$$W = \int_0^i \psi(\theta, i)di \tag{10}$$

The electromagnetic torque T in terms of the co-energy represented as a function of rotor position and phase current is

$$T = \frac{\delta W_m}{\delta\theta} = \frac{\partial \int_0^i \psi(i,\theta)\,\mathrm{d}i}{\partial\theta} = \frac{\partial \int_0^i L(i,\theta) i\,\mathrm{d}i}{\partial\theta} \tag{11}$$

In conclusion, once the flux linkage versus *i* and θ is profiled, all the other electromagnetic properties of an SRM can be hereby deduced.

2.2. Distinct inductance models

We read from Eq. (2) that the excitation current and the flux linkage define an inductance in an instantaneous status, which partially reflects the stationary behavior of the winding impedance. However, when both the dynamic and the stationary inductive characteristics are to be discussed, two distinct models, namely the phase self-inductance *L* and the incremental inductance l need to be derived.

Differentiate Eq. (2), we note that

$$\frac{d\psi(i,\theta)}{dt} = L(i,\theta)|_{\theta=const}\frac{di}{dt} + i\frac{dL(i,\theta)}{dt}|_{i=const} \tag{13}$$

Alternatively,

$$\frac{\mathrm{d}\psi(i,\theta)}{\mathrm{d}t} = \frac{\partial\psi(i,\theta)}{\partial i}\frac{\mathrm{d}i}{\mathrm{d}t} + \frac{\partial\psi(i,\theta)}{\partial\theta}\frac{\mathrm{d}\theta}{\mathrm{d}t} = l(i,\theta)\frac{\mathrm{d}i}{\mathrm{d}t} + \frac{\partial\psi(i,\theta)}{\partial\theta}\omega \tag{14}$$

where

$$l(i,\theta) = \frac{\partial\psi(i,\theta)}{\partial i} = \frac{\partial \int_0^\tau (u - Ri)\,\mathrm{d}t}{\partial i} \tag{15}$$

Meanwhile, the relationship between two representations of phase inductive behavior is

$$L(i,\theta) = \frac{1}{i}\int_0^i l(i,\theta)di \tag{16}$$

Note that the self-inductance is different from the incremental inductance when the operating condition is not linear, which is usually the case in an SRM drive system. It can be further disserted that only the incremental inductance can be used to evaluate the dynamic inductive characteristics such as in an algorithm for position sensorless control (Cai and Deng, 2012; Cai and Deng, 2013). Two inductance models can be mutually converted by Eq. (16). Hence in the following sections, only the phase inductance is analyzed unless there is any need to discriminate them.

3. In-situ characterizing approach

Zhang et al. (Zhang et al., 2010) proposed a current saturation method for accurately measuring the SRM inductance, which uses low frequency and low voltage to minimize the machine loss. Although this measuring setup is simple, unfortunately the proposed solution is not suitable for high-power SRMs up to multiple hundred KW power ratings. In this section we utilize a COTS SRM control circuitry and half-bridge power converter to conduct the measurement, which means the commercially available switched reluctance drive can be used without requiring additional measuring apparatus. A decaying current method is employed to facilitate the high power SRM characterization.

Both COTS SRM development kits and industrial application solutions are extensively provided by semiconductor manufacturers such as Fairchild, Infineon, and Texas Instrument that offer supports not only for the independent central control units, power converters, and integrated motor drivers but also for the comprehensive solution (DiRenzo, 2000). A general-purpose SRM drive circuit is shown in Fig. 1. The A.C. power source is rectified and filtered to provide a D.C. bus voltage, the power switches (IGBTs) S and diodes D are integrated modules to form a compact asymmetry half bridge power converter for SRM. Take Phase A for an example, when S_1 and S_2 are switched on simultaneously, the phase winding is excited by the D.C. source up to rated current, which is limited by a comparing circuitry associated with the COTS SRM drive component. When S_1 and S_2 are switched off, the current decreases.

The SRM electromagnetic characteristics measurement is based on the voltage equation of the SRM in terms of the phase current and flux linkages. As mentioned in previous section, to obtain the parameters for various positions, this experiment can be repeated by applying a pulse voltage in one phase for various locked rotor positions ranging from the aligned to the unaligned position of the stator and rotor poles. Thereby the three-dimensional relationship of $\psi(\theta,i)$ vs. *i* vs. θ can be plotted. This is sufficient for the evaluation of magnetic co-

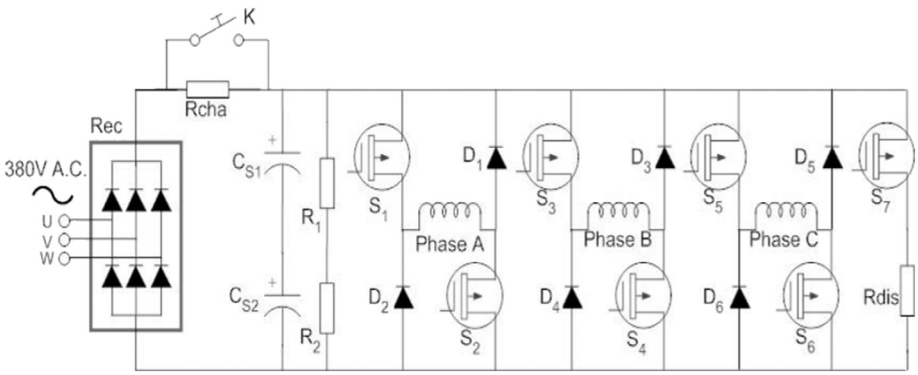

Fig. 1. Asymmetry half-bridge power converter for SRMs.

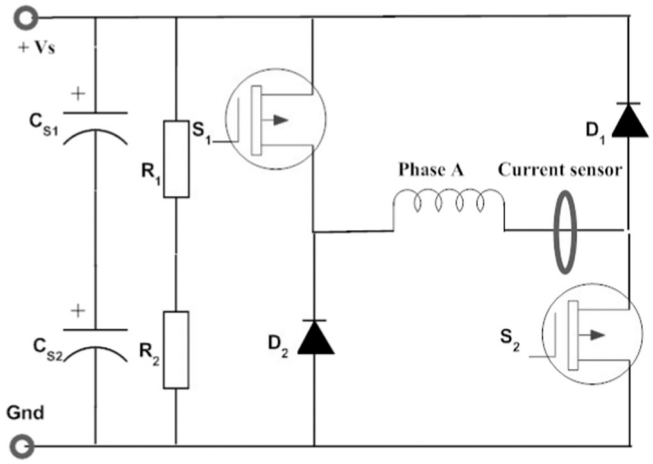

Fig. 2. Asymmetry half-bridge power converter for SRMs.

energy and instantaneous electromagnetic torque for any given current and rotor position. A schematic diagram for measurement is shown in Fig. 2.

The measurement could be conducted by monitoring either rising or decaying current in the phase windings. Clearly, Eq. (1) describes a magnetizing process when the current flow as "+Vs-S_1-Phase A-S_2-Gnd" while the demagnetizing current along "Gnd-D_2-Phase A-D_1-+V_s". theoretically,

$$-u = Ri + \frac{\mathrm{d}\psi(i,\theta)}{\mathrm{d}t} \tag{17}$$

here using the decaying current profile is more appropriate for higher currents since the voltage fluctuation during a falling current is negligible and fairly constant (Gobbi et al., 2006). This is because the measurement during a decaying current is carried out by eliminating the applied voltage to the winding, and an alternative path to the winding current is provided through a freewheeling diode connected across the machine phase, hence no current drains from the filter capacity. The voltage across the winding during the decaying current is only the forward voltage drop of the diode. In contrast, the applied source voltage varies while the current is increasing, giving rise to errors due to quantization and its use in the evaluation of flux linkages (Krishnan, 2001).

The manner in which the flux linkage is obtained is crucial to the accuracy and application of the results. Generally speaking, the proposed characterization method offers three advantages. First, its technical merits and practical value of using the COTS based experimentation setup lie in easily characterizing high-power motors and performing the real application in-system testing. The readily-equipped power convert avoids customizing a specific high power source, and the installed Hall current sensor directly measures the excitation current and eliminates the need for a high power rating data-acquiring precise resistor. Further the phase current limitation is reliably curbed by using an on-board protective circuitry. Therefore, the COTS circuit based experimentation leads to a paradigm shift from laboratory prototyping to manufacturer on-site characterization. Second, using the decaying current to characterize the SRMs ensures a high accuracy via minimizing the voltage fluctuation. Third, although the iron/copper losses and phase mutual inductance complicate the measurement of the electromagnetic properties, the proposed method is capable of genuinely revealing the properties since it realistically duplicates the operating scenario in converter, such as the current path and individual component loss. Therefore, the proposed method can be applied in characterizing a wide spectrum of SRMs.

4. Implementation and experimental results

4.1. Experimental setup

On an 8/6 SRM with the rated power of 750 W and 310 V D.C. bus voltage, a COTS power converter is connected in a half-bridge topology. Figs. 3 and 4 show the photographs of the experimental platform and control circuitry respectively. And refer to the appendix for the detailed parameters of the motor.

In the SRM control board the instantaneous maximum phase current is limited to 13.0A during test, and the maximum current during motor operation is 9.0A. The current sensor is LEM HMS 05-P with the accuracy of 1%. The encoder is OMRON E6C2-C with the resolution of 2000 pulse/round. The general controller is a 32-bit 150MIPS TMS320LF2812 DSP which includes a 16-channel 12-bit on-chip 3D converter with the 12.5 M sampling bandwidth. An Altera FPGA EP2C8Q208C8 (8 speed grade) is selected to expand the I/O and execute online CMAC NN computation, which has 8256 logic cells and 165,888 memory bits. Meanwhile the FPGA has a 16 M byte SDRAM for temporarily reserving the sensor-acquired data.

4.2. Experimentation of characterizing an SRM

For characterizing an SRM the proposed decaying current method applies a D.C. voltage with given width at each rotor position. The time span of the voltage pulse is determined by the current's rising to the maximum. Fig. 5 demonstrates a rising and decaying current slope when a 700us pulse voltage is applied at certain rotor position. By this means the phase current will reach its maximum at all the rotor positions, which enable the characterization covers the entire motor operating regime. The decaying stage is recorded for characterizing the SRM. As can be noticed the current shape is not absolutely symmetry due to the machine loss and bus voltage fluctuation.

Since the mechanical period of an 8/6 SRM is 60° for each phase, the measurements starts from the rotor/stator completely unaligned position −30° and terminates at +30° by 1° interval. The 0° position hints the rotor and stator are strictly aligned. Technically an interpolation algorithm is utilized to obtain fine granular I and θ mesh, and finally we obtain the θ [−30°, 30°] with 0.3° resolution and the current [0A,9.0A] with 0.045A interval. Hence the input set fields are divided into a 201 × 201 mesh, which means a mapping that uses a table looking-up algorithm will require at least 161,604 byte memory cells for 40,401 single precision floating point data storage. The amount of memory occupation indicates the direct table looking-up is not suitable for obtaining multiple parameters in embedded control system, which necessitates a model-based algorithm to solve this problem.

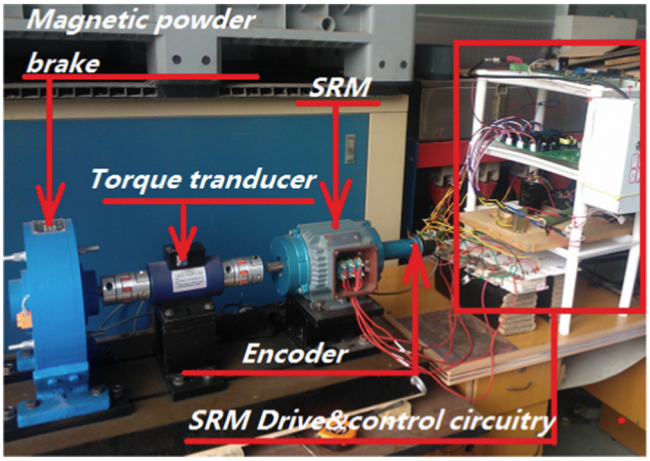

Fig. 3. Experimental system of an SRM.

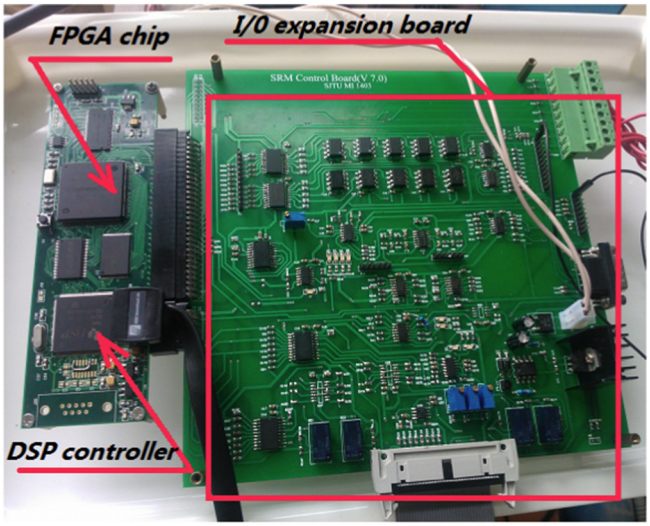

Fig. 4. Control and drive circuitry for the SRM with DSP and FPGA processors

According to the equations established in Section 1, the electromagnetic properties can be characterized. Figs. 6–9 render the 3-D relationship among the variables θ, I and flux linkage ψ, phase inductance L, magnetic co-energy W, electro torque T respectively.

4.3. Cross-validating the characterization result

Traditionally we often resort to an FEM-based approach to validate the testing result, which is dubious due to the errors induced by mismatches between simulation parameters and the real case.

In order to validate the effectiveness and accuracy of the characterization, two aspects are considered in this paper. First, decaying current is used to characterize the incremental inductance and at the same position the rising current is used to validate its result. This approach is name after cross-validation because both the currents are shapes by the identical inductance regarding to the fixed position. The second aspect is that a numerical model is built according to the decaying current model and then a full process is simulated and experimentally recorded to show their agreement.

At a randomly selected rotor position 41.3066°, a 1100 μs pulse voltage is applied so as to allow the phase current approach its maximum. The voltage width and the phase current response are recorded to

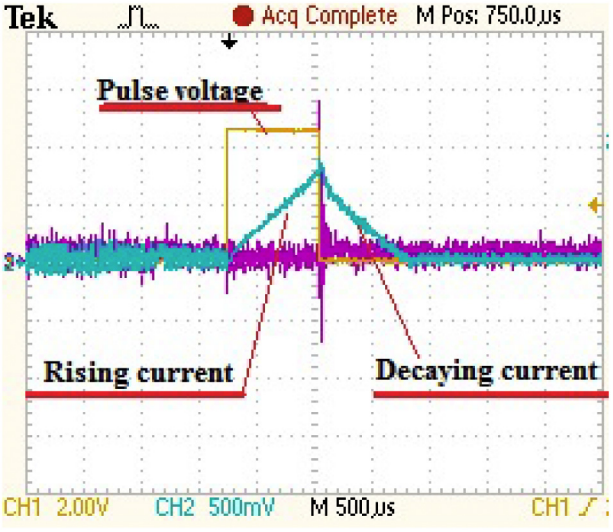

Fig. 5. Phase current profile when a pulse voltage is applied.

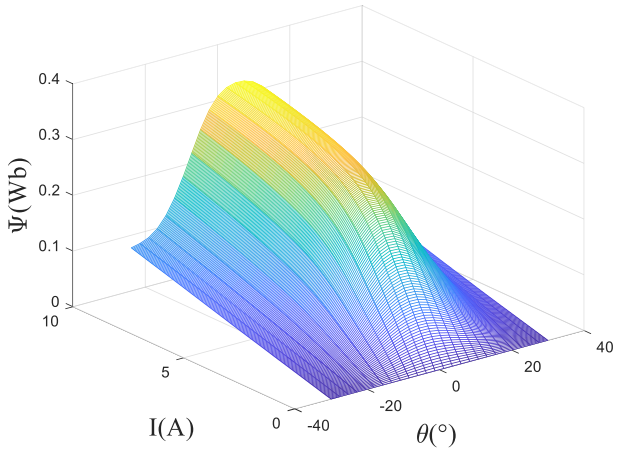

Fig. 6. Linkage flux as a function of the rotor position and the phase current.

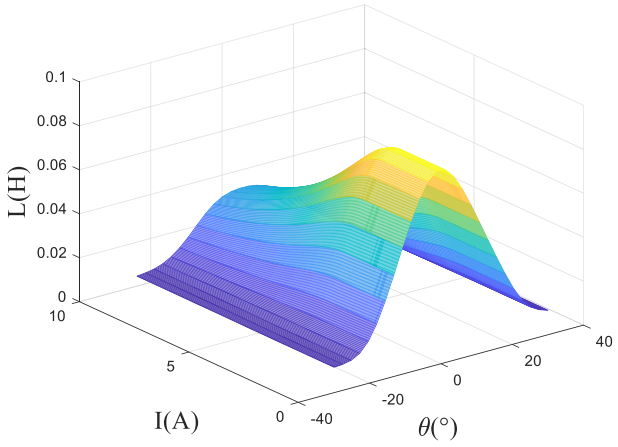

Fig. 7. Inductance as a function of the rotor position and the phase current.

perform the simulation. On the basis of the flux linkage characterization shown in Fig. 6, the excitation current profile is generated accordingly.

The simulation MATLAB/SIMULINK procedure is shown in Fig. 10, and the experimentally measured current profile and the simulation result are compared in Fig. 11. Fig. 11 shows that the simulated phase current response to a fixed voltage pulse matches the measured current, and it proves that the electromagnetic properties characterization are accurate at the full spectrum of current and rotor position. The current

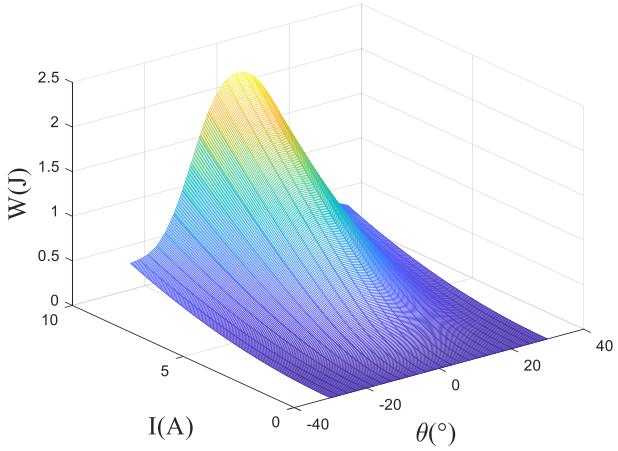

Fig. 8. Magnetic co-energy as a function of the rotor position and the phase current.

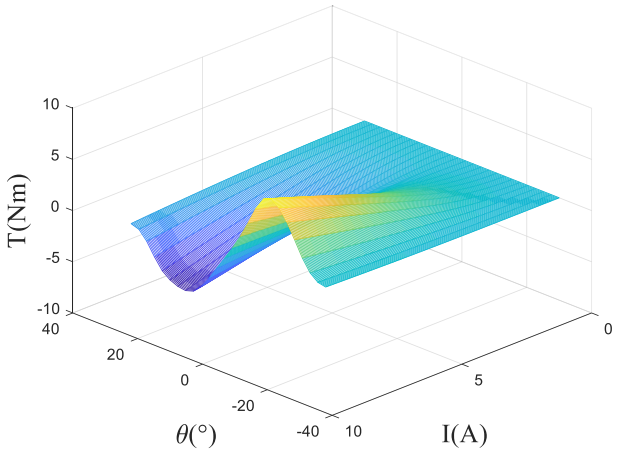

Fig. 9. Electromagnetic torque as a function of the rotor position and the phase current.

plateau at 9A embodies the overcurrent chopping effect in the protection circuit.

Clearly, this in-situ validation approach can be conducted immediately after the characterization process, and the results can be evaluated by simply check the agreement of two one dimensional curves.

5. Conclusion

The proposed methodology, including both of the characterization and verification techniques for SRMs, opens up the possibility of precisely calculating its electromagnetic characteristics in real time, which lays a foundation stone for versatile advanced control schemes that require obtaining accurate electromagnetic parameters in corresponding models. A model-based in-situ measuring system instrumented in COTS platform enables fast, applicable machine-by-machine characterization in a massive production line of the motor manufacturers, which can be easily involved in an existing infrastructure. Experimental results proved that the proposed method could achieve an encouraging performance. Conclusions are listed as follows.

1) The proposed measuring approach utilize the off-the-shelf devices and circuitry to support in-factory SRM test and characterization, easing the burden of developing an ad hoc test bench and possessing the ability of including all physical effects that exist in the real application.
2) The precisely measured electromagnetics data and established model enable detailed and precise examination of SRM behavior over a wide variety of simulated operating conditions without the limitations associated with drive circuits, transducers or instrumentation, as the case we used for validating the characterization precision in Section 4.2. And it worth noting that all the electromagnetic parameters are able to be manipulated under a unified computational framework.

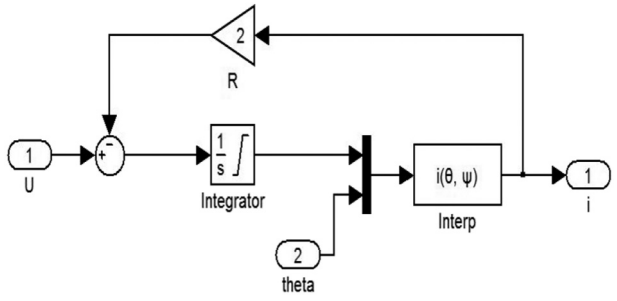

Fig. 10. MATLAB/Simulink procedure for simulating the phase current response to a voltage pulse.

3) Highly reliable cross validation methodology is proposed for verifying the in-situ characterization result, which does not need any specifically design instrument either.

CRediT authorship contribution statement

Xiao Ling: Conceptualization, Data curation, Formal analysis, Methodology, Validation, Writing - original draft.**Liang Gong:**Data curation, Formal analysis, Investigation, Methodology, Validation, Writing - original draft, Writing - review & editing.**Bingchu Li:**Data curation, Methodology, Validation.**Chengling Liu:**Funding acquisition, Project administration, Visualization, Writing - review & editing.

Acknowledgements

The authors gratefully acknowledge the financial support provided by the National Natural Science Foundation of China (project No. 11202125 and project No. 51305258).

Appendix A

Motor data:
Number of phases 4;
Number of rotor poles 6;
Rated power 750 W;
Rated torque 5.0 N m;
Maximum speed 1500 r/min;
Phase current limitation 9A;
Design specification of the aligned phase inductance 22 mH;
Design specification of the unaligned phase inductance0.5 mH;
Phase resistance 1.3 Ohm
Bus D.C. voltage 300 V;
Lamination material: M19 steel

References

Brauer, H.J., Hennen, M.D., De Doncker, R.W., Jan. 2012. Control for polyphase switched reluctance machines tominimize torque ripple and decrease ohmic machinelosses. IEEE Transactions on Power Electronics 27 (1), 370–378.

Cai, J., Deng, Z.Q., Jul. 2012. Sensorless control of switched reluctance motor based on phase inductance vectors. IEEE Transactions on Power Electronics 27 (7), 3410–3423.

Cai, J., Deng, Z.Q., Mar., 2013. A position sensorless control of switched reluctance motors based on phase inductance slope. Journal of Power Electronics 13 (2), 264–274.

Cheok, A.D., Fukuda, Y., Apr. 2002. A new torque and flux control method for switched reluctance motor drives. IEEE Transactions on Power Electronics 17 (4), 543–557.

DiRenzo, Michael T., Feb., 2000. Switched Reluctance Motor Control – Basic Operation and Example Using the TMS320F240. Tech. Memo.spra420a*Texas Instruments Inc.*, Austin.

Dowlatshahi, M., Saghaiannejad, S.M., Ahn, J.W., et al., Mar. 2014. Copper loss and torque ripple minimization in switched reluctance motors considering nonlinear and magnetic saturation effects. Journal of Power Electronics 14 (2), 351–361.

Gobbi, R., Sahoo, N.C., Rajandran, R. Vejian, 2006. Rising and falling current methods for measurement of flux-linkage characteristics of switched reluctance motors: a comparative study. Proc.of IEEE PECON'06, pp. 383–387.

Goto, H., Nishimiya, A., Guo, H.J., Jan. 2010. Instantaneous torque control using flux-based commutation and phase-torque distribution technique for SR motor EV. COMPEL-International Journal for Computation and Mathematics in Electrical and Electronic Engineering 29 (1), 173–186.

Kamalakannan, C., Kamaraj, V., Paramasivam, S., Paranjothi, S.R., *2011*. Switched reluctance machine in automotive applications — a technology status review. Proc. ICEES, pp. 187–197.

Kjaer, P.C., Nielsen, P., Andersen, L., Blaabjerg, F., May 1995. A new energy optimizing control strategy for switched reluctance motors. IEEE Transactions on Industry Applications 31 (5), 1088–1095.

Krishnan, R., 2001. In: Irwin, J.D. (Ed.), Switched Reluctance Motor Drives: Modeling, Simulation, Analysis, Design, and Applications. Boca Raton, London New York Washington, D.C.

Lee, D.H., Ahn, S.Y., Ahn, J.W., Jan. 2012. A simple negative torque compensation scheme for a high speed switched reluctance motor. Journal of Power Electronics 12 (1), 58–66.

Miller, T.J.E., 2001. Electronic Control of Switched Reluctance Machines. Newnes D.C, Burlington MA,USA.

Moron, C., Garcia, A., Tremps, E., Apr 2012. Torque control of switched reluctance motors. IEEE Trans. Magn. 48 (4), 1661–1664.

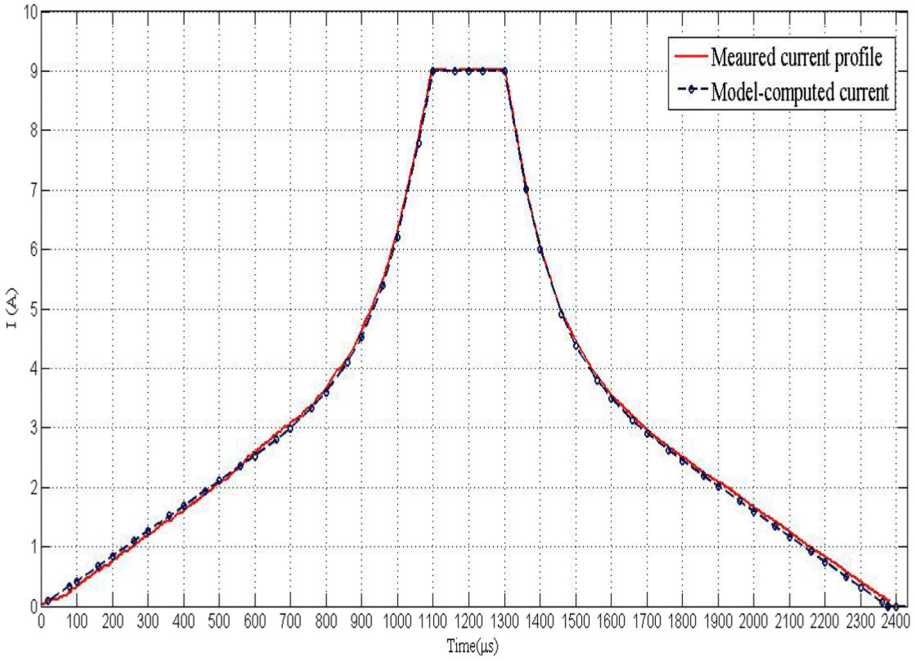

Fig. 11. A comparison between the measured current and the model-generated current.

Parreira, B., Rafael, S., Pires, A.J., Branco, P.J. Costa, Jun. 2005. Obtaining the magnetic characteristics of an 8/6 switched reluctance machine: from FEM analysis to the experimental test. IEEE Transactions on Industrial Electronics 52 (6), 1635–1643.

Shin, D.S., Li, Y.C., Yang, H.Y., et al., Mar. 2005. Rotor position sensing method for switched reluctance motors using an indirect sensor. Journal of Power Electronics 5 (3), 173–179.

Vujicic, P. Vladan, Jan. 2012. Minimization of torque ripple and copper losses in switched reluctance drive. IEEE Transactions on Power Electronics 27 (1), 388–399.

Wang, B., Lee, D.H., Lee, C.W., et al., Sep. 2014. Characteristics analysis of a novel segmental rotor axial field switched reluctance motor with single teeth winding. Journal of Power Electronics 14 (5), 852–858.

Wen, D., Liu, L., Lou, J.Y., Mar 2013. Design and control of a high-speed switched reluctance machine with conical magnetic bearings for aircraft application. IET Electronic Power Applications 7 (3), 179–190.

Wong, K.F., Cheng, K.W.E., Ho, S.L., Mar 2009. Four-quadrant instantaneous torque control of switched reluctance machine at low speed based on co-energy control. IET Electronic Power Applications 3 (5), 431–444.

Yoo, A., Sul, S.K., Lee, D.C., Jun, C.S., Dec 2009. Novel speed and rotor position estimation strategy using a dual observer for low-resolution position sensors. IEEE Transactions on Power Electronics 24 (12), 2897–2906.

Yu, S.Y., Feng, F.G., Lee, D.H., et al., Jan. 2015. High efficiency operation of a switched reluctance generator over a wide speed range. Journal of Power Electronics 15 (1), 123–130.

Zeng, H., Chen, Z., Chen, H., Mar. 2014. Smooth torque speed characteristic of switched reluctance motors. Journal of Power Electronics 14 (2), 341–350.

Zhang, P., Cassani, P.A., Williamson, S.S., Sept. 2010. An accurate inductance profile measurement technique for switched reluctance machines. IEEE Transactions on Industrial Electronics 57 (9), 2972–2979.